*Int. J. Electrochem. Sci.*, 11 **(2016)** 5655 – 5668, doi: 10.20964/2016.07.57

International Journal of
ELECTROCHEMICAL
SCIENCE
www.electrochemsci.org

# Effect of Pretreatment and Annealing on Aluminum Coating Prepared by Physical Vapor Deposition on AZ91D Magnesium Alloys

*Fan Liu*[3], *Xu Chen*[3], *Yuekun Gu*[1], *Chao Ma*[1], *Xiaopeng Han*[2], *Yida Deng*[2], *Wenbin Hu*[1,2,3], *Cheng Zhong*[1,2,*]

[1] Key Laboratory of Advanced Ceramics and Machining Technology (Ministry of Education), School of Materials Science and Engineering, Tianjin University, Tianjin 300072, China
[2] Tianjin Key Laboratory of Composite and Functional Materials, School of Materials Science and Engineering, Tianjin University, Tianjin 300072, China
[3] State Key Laboratory of Metal Matrix Composites, Department of Materials Science and Engineering, Shanghai Jiao Tong University, Shanghai, 200240, China (The first and second authors contributed equally)
[*]E-mail: cheng.zhong@tju.edu.cn

*Received:* 10 April 2016 / *Accepted:* 18 May 2016 / *Published:* 4 June 2016

Magnesium alloys have been widely used in many fields owing to its light weight. However, their poor corrosion resistance has prevented their further applications. In this study, vacuum evaporation deposition coupled with the pretreatment of the AZ91D magnesium alloy substrates were employed to successfully prepare an aluminum coating on AZ91D magnesium alloy in an attempt to enhance its corrosion resistance. The surface morphology, corrosion resistance and adhesive strength of the coatings prepared from different pretreatments were systemically investigated. The effect of deposition time and annealing treatment on the surface morphology, corrosion resistance and adhesive strength was also examined. The results showed that the best corrosion resistance and highest adhesive strength of the aluminum coating were obtained for the specimen pretreated by $H_3PO_4$ etching. As the deposition time increases, a continuous and dense aluminum coating gradually forms on the surface of magnesium alloy following the typical island growth (Volmer-Weber) mode. The increase of deposition time enhances the corrosion resistance of magnesium alloy but has no effect on the adhesive strength between the coating and the substrate. With the increase of the annealing temperature, the coating of the sample becomes more uniform with better crystallinity of aluminum compared with unannealed sample.

**Keywords:** Magnesium alloy; Vacuum evaporation deposition; Pretreatment; Annealing; Corrosion resistance

## 1. INTRODUCTION

There is an ever increasingly urgent need to reduce the environmental pollution and tackle the energy crisis, magnesium has become the ideal material concerning this background [1-3]. The magnesium and its alloys possess not only low density but also high strength [4]. Apart from the high strength/weight ratio, magnesium and its alloys also share a combination of great castability, great machinability and easy recycling procedures, which makes them the green material of the new century [2]. Such unique properties have broaden the industrial applications of magnesium alloys, nowadays they are widely used in the aerospace, electronic and automobile industries [5]. However, the key drawback of magnesium and its alloys is the low corrosion resistance, limiting their further applications [2-4, 6, 7]. The standard electrode potential of magnesium $E^0_{mg^{2+}/mg}$ is –2.37 V and the magnesium alloys are susceptible to galvanic corrosion as well as pitting corrosion [6, 8], which makes their corrosion behavior a major concern.

An effective method to improve the poor corrosion resistance of magnesium alloys is to coat the substrate through surface treatment [9, 10]. Surface modification in a way of coating has become an essential process to improve the surface properties in terms of wear, corrosion and oxidation. Typical surface treatment techniques include anodizing [11-14], chemical conversion coatings [15-17], diffusion coatings [18-22], electrodeposition [23-27], laser surface alloying [28] and flame spray [29]. Among the aforementioned techniques, physical vapor deposition (PVD) technology has drawn increasing attention because it's environmental friendly and the formed coating is of high quality [1, 9, 10]. The PVD coatings on the magnesium alloys can be categorized into ceramic coatings [2, 4, 30, 31] and metal coatings [32-37]. The metal coatings (e.g., Al and Ti) exhibit good corrosion resistance in aggressive environments [32]. Al especially is the main composition of magnesium alloys and possesses the ability to self-repair corrosion [28]. In the PVD techniques, Al coatings are mostly prepared from magnetron sputtering and the vacuum evaporating deposition has been discussed less often. The effect of annealing process on the coatings has been addressed frequently in the application of PVD techniques [34] as well as other techniques [38-40], however, the pretreatment of the magnesium alloy substrate has been rarely investigated in the PVD technique. The surface pretreatment of the substrate is essential to ensure the adhesion and integrity of the coatings in the corrosive environment [41]. Therefore, it is highly required to investigate the effect of the pretreatment on the properties of the PVD coatings on magnesium alloys.

In the present work, vacuum evaporating deposition coupled with the pretreatment of the magnesium alloy substrate were employed to successfully prepare an aluminum coating on AZ91D magnesium alloy in an attempt to enhance its corrosion resistance. The surface morphology, corrosion resistance and adhesive strength of the specimens prepared from different pretreatments (mechanical polishing and different acid etching) were systemically investigated. The effect of deposition time and annealing treatment on the surface morphology, corrosion resistance and adhesive strength of the coatings was also examined.

## 2. EXPERIMENTAL

### *2.1. Preparation of aluminum coating on AZ91D magnesium alloy*

The aluminum wire with high purity (99.99%) was used as the metal source for the vacuum evaporation deposition of aluminum coating on AZ91D magnesium alloys. Pretreatments on AZ91D magnesium substrates were applied to investigate its effect on the corrosion resistance of the PVD aluminum coating on magnesium alloys. Basic pretreatment includes mechanical polishing: the AZ91D magnesium alloy substrates were cut into pieces (50 mm×10 mm×1 mm) and then were ground with abrasive paper up to 1200 grit, cleaned by distilled water and ethanol. After the mechanical polishing pretreatment, the samples were further etched with 0.1 mol $L^{-1}$ HCl solution, 0.5 mol $L^{-1}$ $H_2SO_4$ solution, 10 wt.% oxalic acid solution, 85 wt.% $H_3PO_4$ solution and 10 wt.% $H_3PO_4$ solution, respectively. The etching time was 15 s and then the substrates were cleaned by distilled water and ethanol.

The vacuum evaporation deposition was achieved through a vacuum evaporation coating machine (HUS-5GB). The deposition process only starts as the degree of vacuum decreases below $10^{-4}$ Pa. The deposition time was chosen as 3 min, 6 min and 9 min, respectively.

To further investigate the effects of annealing process on the morphology, the adhesive strength and corrosion resistance of the aluminum film, the vacuum annealing process of the as-prepared samples was achieved in a vacuum furnace (Hefei Kejing materials technology Co., Ltd). The annealing time was chosen as 1 h and annealing temperature was 200 °C and 400 °C, respectively.

### *2.2. Experimental measurement*

#### *2.2.1 Surface characterizations*

The surface morphology of specimen was characterized by a SEM (JEOL JSM-7600) and the composition of elements in the coating was detected by energy dispersive spectrometer (EDS, X-Max, Oxford, England). The phase analysis of the coating after vacuum annealing process was conducted by X-ray diffraction (D/Max 2550V).

#### *2.2.2 Adhesive strength characterization*

The adhesive strength between the aluminum coating and the AZ91D alloy substrate was characterized according to ASTM D3359-1997 standard (cross-cut tape test) [42]. The adhesive strength was measured by the grid area for removal of coating from the substrate and could be categorized into 6 grades.

#### *2.2.3 Corrosion resistance characterization*

The corrosion resistance of the aluminum coating was characterized by AC impedance curve and Tafel curve using an electrochemical workstation (CHI 660E). The as-prepared samples were

immersed in 3.5 wt.% NaCl solution to simulate the corrosive environment. The alloy samples were used as working electrode (WE), a saturated calomel electrode (SCE) as the reference electrode (RE) and a Pt electrode as the counter electrode (CE). Firstly the alloy samples were immersed in 3.5 wt.% NaCl solution for 400 s to stabilize the open circuit potential. The frequency in the AC impedance test was between 0.01 and 100000 Hz, and the obtained open circuit potential was chosen as the initial corrosion potential. In the Tafel test, the corrosion potential was chosen between –1.8 V and –1.2 V, and the scan rate was 1 mV $s^{-1}$. All tests were performed at room temperature (~25 °C).

## 3. RESULTS AND DISCUSSION

### *3.1. Influence of pretreatment on aluminum coating*

#### *3.1.1 Influence of pretreatment on morphology*

Fig. 1(a)-(f) shows the SEM images of the mechanically polished sample, 0.1 mol $L^{-1}$ HCl etched sample, 0.5 mol $L^{-1}$ $H_2SO_4$ etched sample, 10 wt.% oxalic acid etched sample, 85 wt.% $H_3PO_4$ etched sample and 10 wt.% $H_3PO_4$ etched sample before the deposition of Al, respectively. Special attention should be paid to the morphology of oxalic acid and $H_3PO_4$ etched samples. After etching with oxalic acid, the grain boundary appears and the morphology shows a net-like shape. The morphology of samples varies with the concentration of $H_3PO_4$. Etched with 85 wt.% $H_3PO_4$, a clean and dense phosphate film was formed except for a small amount of holes generated by the corrosion, however, a porous morphology was obtained when etched with 10 wt.% $H_3PO_4$.

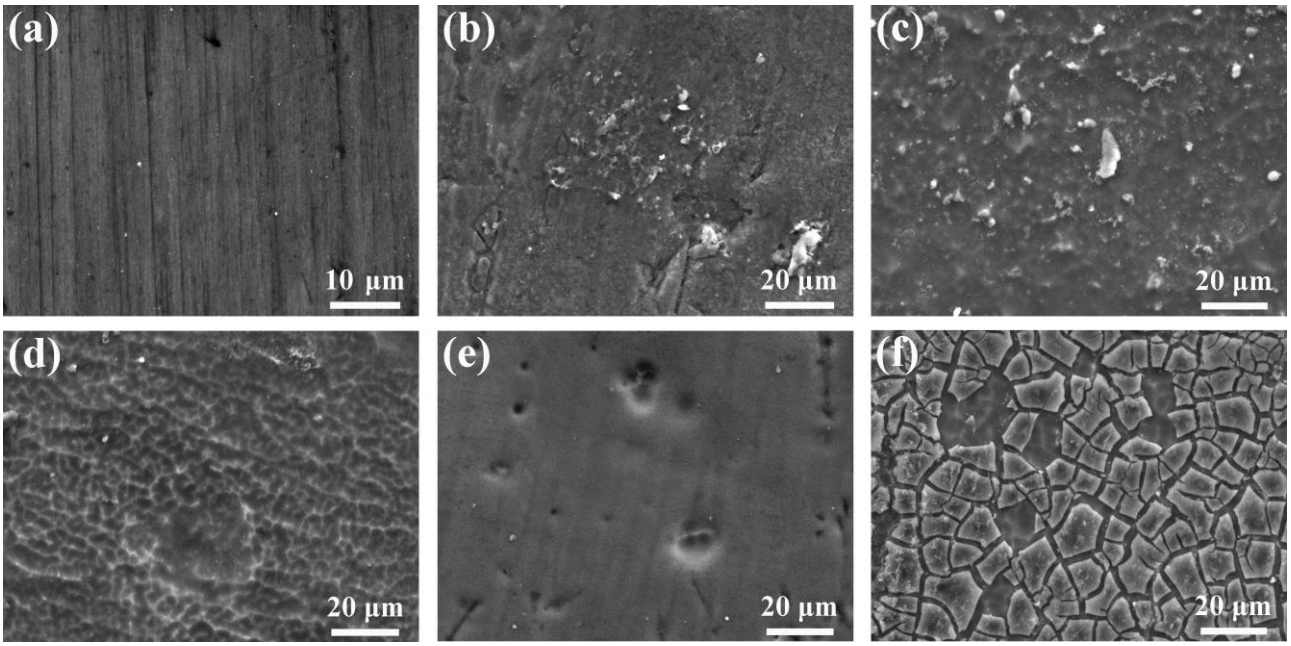


**Figure 1.** SEM images of the (a) mechanically polished sample, (b) 0.1 mol $L^{-1}$ HCl etched sample, (c) 0.5 mol $L^{-1}$ $H_2SO_4$ etched sample, (d) 10 wt.% oxalic acid etched sample, (e) 85 wt.% $H_3PO_4$ etched sample, (f) 10 wt.% $H_3PO_4$ etched sample before the deposition of Al

Fig. 2(a)-(f) shows the SEM images of the mechanically polished sample, 0.1 mol $L^{-1}$ HCl etched sample, 0.5 mol $L^{-1}$ $H_2SO_4$ etched sample, 10 wt.% oxalic acid etched sample, 85 wt.% $H_3PO_4$ etched sample and 10 wt.% $H_3PO_4$ etched sample after the deposition of Al, respectively. Compared with Fig. 1(a)-(f), the morphology of the samples after deposition of Al typically involves the Al particles covering on the surface of the substrates. Especially in Fig. 2(d)-(f), Al particles can be clearly seen to fill the pores on the etched substrates. An increase of the ratio of the Al composition (generally from 2% to 14% in molar ratio) reveals the fact that Al has been successfully deposited on the substrates.

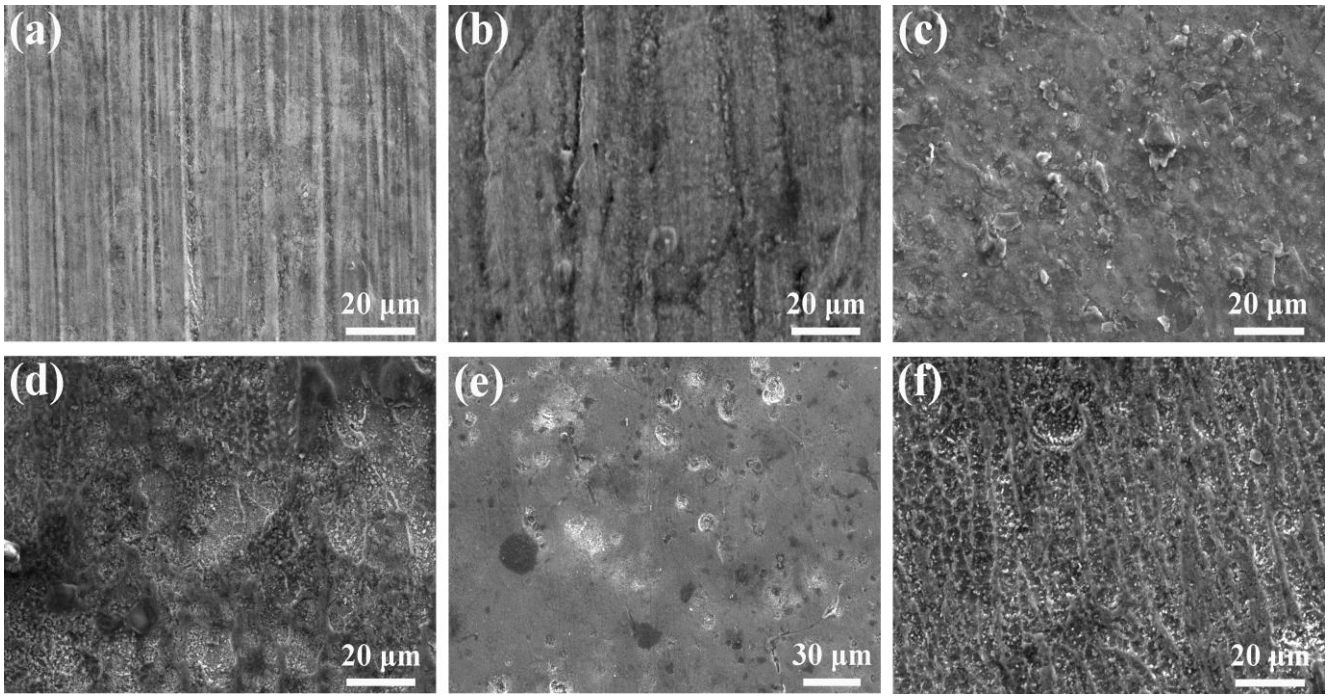


**Figure 2.** SEM images of the (a) mechanically polished sample, (b) 0.1 mol $L^{-1}$ HCl etched sample, (c) 0.5 mol $L^{-1}$ $H_2SO_4$ etched sample, (d) 10 wt.% oxalic acid etched sample, (e) 85 wt.% $H_3PO_4$ etched sample, (f) 10 wt.% $H_3PO_4$ etched sample after the deposition of Al

*3.1.2 Influence of pretreatment on adhesive strength and corrosion resistance*

The adhesive strength between the coating and the substrate under different pretreatment processes is listed in Table 1. Without annealing process, the adhesive strength was generally low regardless of the pretreatment process. However, the samples etched with 10 wt.% oxalic acid and 10 wt.% $H_3PO_4$ exhibit relatively high adhesive strength (grade 1B and 2B, respectively). This could be attributed to the porous morphology shown in Fig. 1(d), (f) and Fig. 2(d), (f). The Al particles deposited in the pores on the substrates could facilitate the serrated interfacial bonding between the Al coating and substrate, thus effectively promoting the adhesive strength through a mechanical riveting effect.

**Table 1.** Adhesive strength of the Al coatings under different pretreatment processes

| Pretreatment process | Percentage of grid area removed | Grade |
|---|---|---|
| mechanical polishing | 82% | 0B |
| etched with 0.1 mol $L^{-1}$ HCl | 85% | 0B |
| etched with 0.5 mol $L^{-1}$ $H_2SO_4$ | 80% | 0B |
| etched with 10 wt.% oxalic acid | 48% | 1B |
| etched with 85 wt.% $H_3PO_4$ | 87% | 0B |
| etched with 10 wt.% $H_3PO_4$ | 20% | 2B |

Fig. 3(a), (b) present the AC impedance curves and Tafel curves of different pretreated samples after the vacuum deposition of Al. The diameter of the capacitive loop in Fig. 3(a) corresponds to the charge transfer resistance. The corrosion rate of the electrode decreases as the diameter of the capacitive loop increases [19]. According to Fig. 3(a), the 10 wt.% $H_3PO_4$ etched sample exhibits the largest diameter which reveals the best corrosion resistance, and the 0.5 mol $L^{-1}$ $H_2SO_4$ etched sample comes the second. Similar conclusion can be drawn from the Tafel curves in Fig. 3 (b). The Tafel curves of 0.5 mol $L^{-1}$ $H_2SO_4$ etched and 10 wt.% $H_3PO_4$ etched samples have obvious passivation region, indicating that corrosion process could be effectively prohibited.

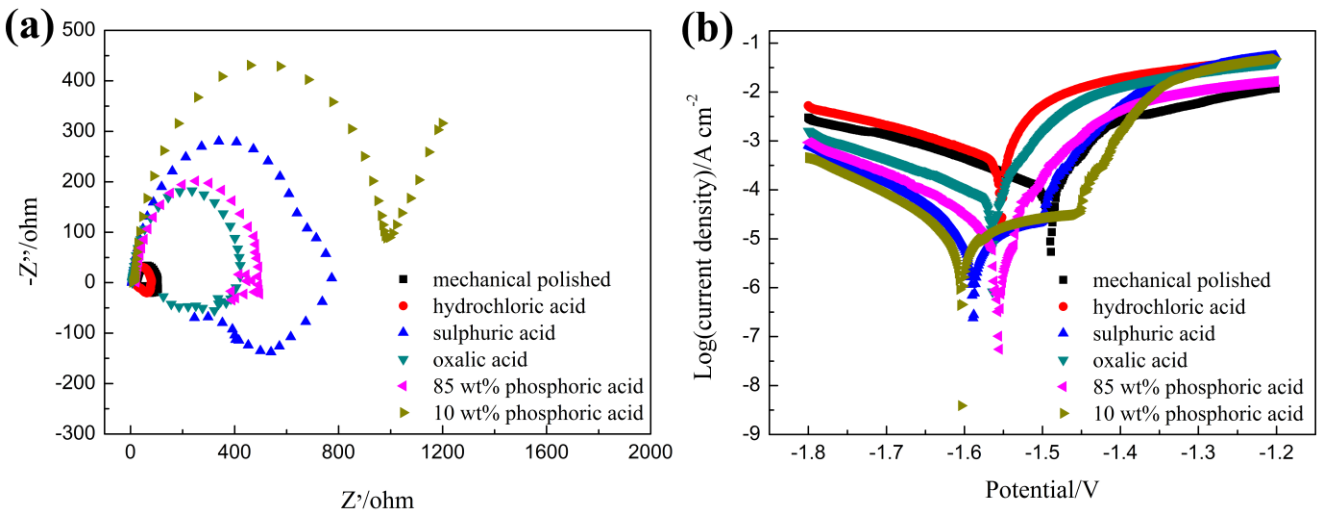


**Figure 3.** (a) AC impedance curves, (b) Tafel curves of different pretreated samples after the vacuum deposition of Al

Table 2 lists the corresponding corrosion parameters (including corrosion potential, the current density and polarization resistance) derived from the Tafel curves and Electrochemical Impedance

Spectroscopy (EIS) by the electrochemical workstation. The results confirm the initial judgment from observing the AC impedance curves and Tafel curves. The samples etched with $H_2SO_4$ and $H_3PO_4$ exhibit better corrosion resistance. However, the best pretreatment process should be chosen as etching with 10 wt.% $H_3PO_4$ when taking the adhesive strength into account. Acid pickling as an effective pretreatment to improve the corrosion resistance of the magnesium alloy has been investigated in conversion and sol-gel coatings [43-45]. It was found that acid pickling already reduces the corrosion of magnesium alloy significantly, conversion and sol-gel coatings based on acid pretreatment further improve the corrosion resistance, which agrees well with our results in PVD coatings.

**Table 2.** Corrosion parameters derived from the Tafel curves

| Pretreatment process | Corrosion Potential/V | Corrosion Current density/A $cm^{-2}$ | Polarization Resistance /Ω |
|---|---|---|---|
| mechanical polishing | -1.488 | $3.54\times10^{-4}$ | 99.5 |
| etched with 0.1 mol $L^{-1}$ HCl | -1.553 | $1.55\times10^{-3}$ | 25.3 |
| etched with 0.5 mol $L^{-1}$ $H_2SO_4$ | -1.588 | $6.59\times10^{-6}$ | 1980.9 |
| etched with 10 wt.% oxalic acid | -1.564 | $1.41\times10^{-4}$ | 171 |
| etched with 85 wt.% $H_3PO_4$ | -1.555 | $7.22\times10^{-6}$ | 2568.2 |
| etched with 10 wt.% $H_3PO_4$ | -1.604 | $1.88\times10^{-5}$ | 1973.8 |

### *3.2. Influence of deposition time on aluminum coating*

#### *3.2.1 Influence of deposition time on morphology*

Based on etching with 10 wt.% $H_3PO_4$ as pretreatment, Fig. 4(a)-(c) shows the SEM images of the samples after deposition for 3 min, 6 min and 9 min, respectively. As can be seen from Fig. 4(a), after deposition for 3 min, the Al atoms deposited on the surface of the substrate gather and grow to form discrete islands through nucleation. The typical morphology of alloy substrate etched by $H_3PO_4$ can still be observed which indicates the discrete islands haven't grown into a dense film. After deposition for 6 min, Fig. 4(b) shows no sign of the alloy substrate, and the discrete islands enlarge and connect to each other, thus forming a percolating network. Fig. 4(c) shows the morphology after deposition for 9 min, the holes on the substrate are covered by the newly deposited Al atoms and a continuous and dense film is formed.

The growth of the aluminum coating on the magnesium alloy substrate follows the typical Volmer–Weber growth mode in vapor deposition [46, 47]. The schematic illustration is shown in Fig. 5 [46]: in a typical Volmer–Weber mode, initially the film is formed and grown after the nucleation of discrete islands which can be seen in Fig. 4(a); the existing islands become larger as the deposition

continues, the new islands can also nucleate to form a continuous percolating network shown in Fig. 4(b); the growth of the film continues until the substrate is fully covered by the deposit shown in Fig. 4(c), followed by the additional film thickening.

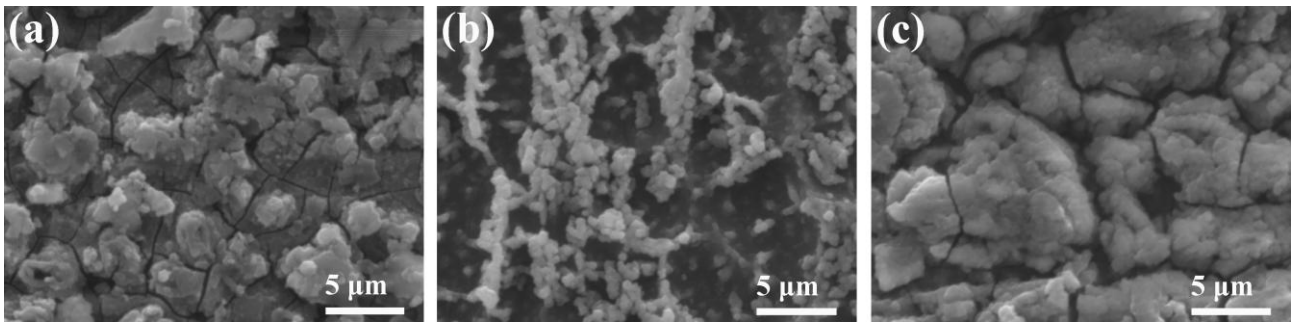


**Figure 4.** SEM images of samples after deposition for (a) 3 min, (b) 6 min, (c) 9 min

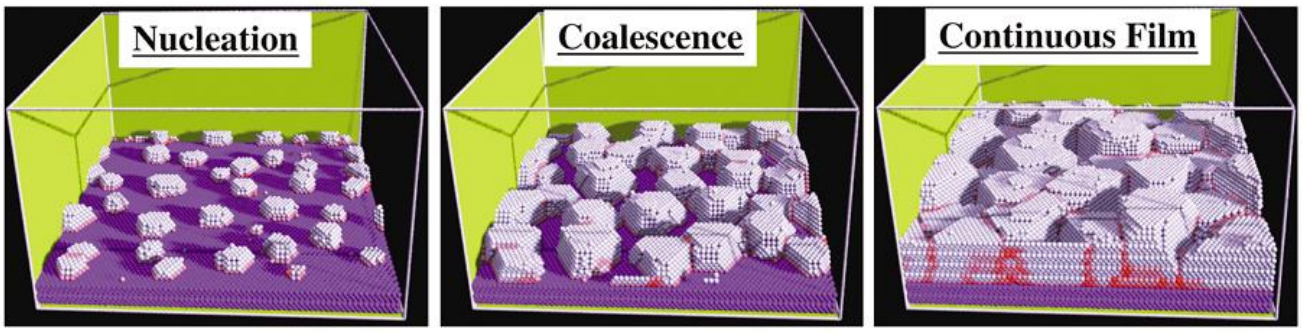


**Figure 5.** The regimes of microstructural evolution during Volmer–Weber growth. Reprinted from Ref. [46], with permission from Cambridge University Press

*3.2.2 Influence of deposition time on adhesive strength and corrosion resistance*

Table 3 lists the adhesive strength between the coating and the substrate under different deposition time, the pretreatment process is chosen as etching with 10 wt.% $H_3PO_4$ since it provides the best adhesive strength of the coating from the previous study. It is obvious that the adhesive strength between the coating and the substrate remains almost the same as the deposition time increases. We can tell that the deposition time or the thickness of the film doesn't necessarily affect the adhesive strength of the coating.

**Table 3.** Adhesive strength of the Al coatings under different deposition time

| Deposition time | Percentage of grid area removed | Grade |
|---|---|---|
| 3 min | 20% | 2B |
| 6 min | 16% | 2B |
| 9 min | 21% | 2B |

Fig. 6(a) and (b) show the AC impedance curves and Tafel curves of the 10 wt.% $H_3PO_4$ etched samples after the vacuum deposition for different time. According to Fig. 6(a), the diameter of the capacitive loop which reveals the corrosion resistance enlarges as the deposition time increases from 3 min to 9 min. The Tafel curves shown in Fig. 6(b) also prove the aforementioned conclusion. The corrosive current density derived from Tafel curves decreases from $4.4\times10^{-5}$ A $cm^{-2}$ to $2.4\times10^{-5}$ A $cm^{-2}$ and finally to $2.6\times10^{-6}$ A $cm^{-2}$ as the deposition time increases from 3 min to 6 min and at last to 9 min. The corresponding polarization resistance also increases from 440.6 Ω to 1612.3 Ω and finally to 3160.4 Ω accordingly. The Tafel curves of samples deposited for 6 min and 9 min have obvious passivation region, which means that the corrosive behavior could be effectively prohibited.

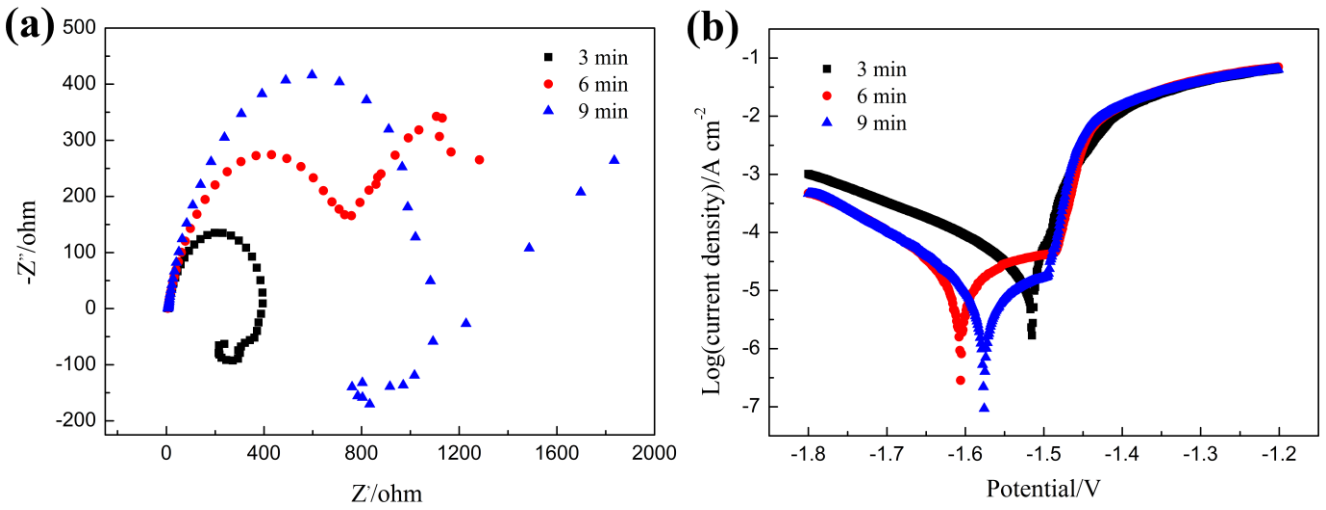


**Figure 6.** (a) AC impedance curves, (b) Tafel curves of the 10 wt.% $H_3PO_4$ etched samples after the vacuum deposition for different time

### *3.3. Influence of annealing process on aluminum coating*

#### *3.3.1 Influence of annealing process on morphology*

In order to improve the adhesive strength between the aluminum coating and the substrate, annealing process is introduced and its effect on morphology is also investigated. Based on etching with 10 wt.% $H_3PO_4$ as pretreatment, Fig. 7(a)-(c) shows the SEM images of the samples after deposition for 9 min without annealing, with annealing at 200 °C for 1 h and with annealing at 400 °C for 1 h, respectively. Compared with the sample without annealing in Fig. 7(a), samples with annealing in Fig. 7(b)-(c) are obviously featured with different morphologies. In Fig. 7(b), a continuous percolating network is formed with annealing at 200 °C for 1 h. As the annealing temperature increases to 400 °C, the morphology in Fig. 7(c) is comprised of well-distributed aluminum particles and the alloy substrate etched by 10 wt.% $H_3PO_4$ disappears compared with Fig. 7(b), which can be ascribed to the diffusion of Al on the magnesium alloy substrate.

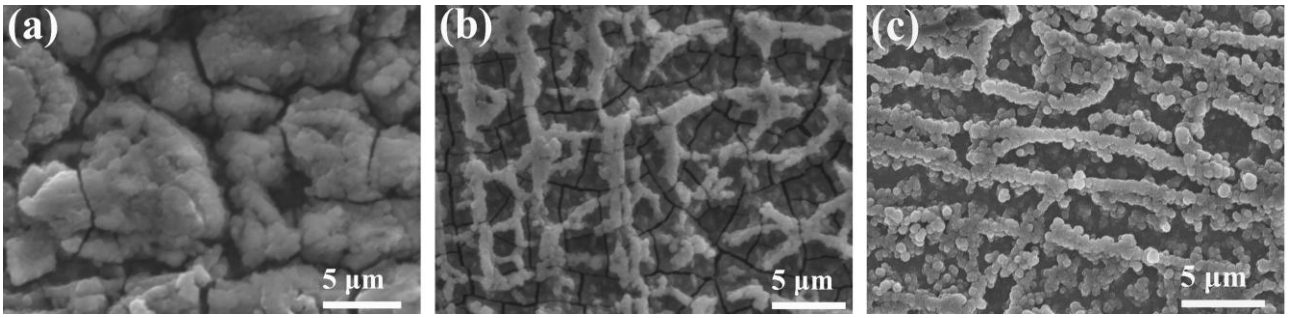


**Figure 7.** SEM images of the samples after deposition for 9 min (a) without annealing, (b) with annealing at 200 °C for 1 h, (c) with annealing at 400 °C for 1 h

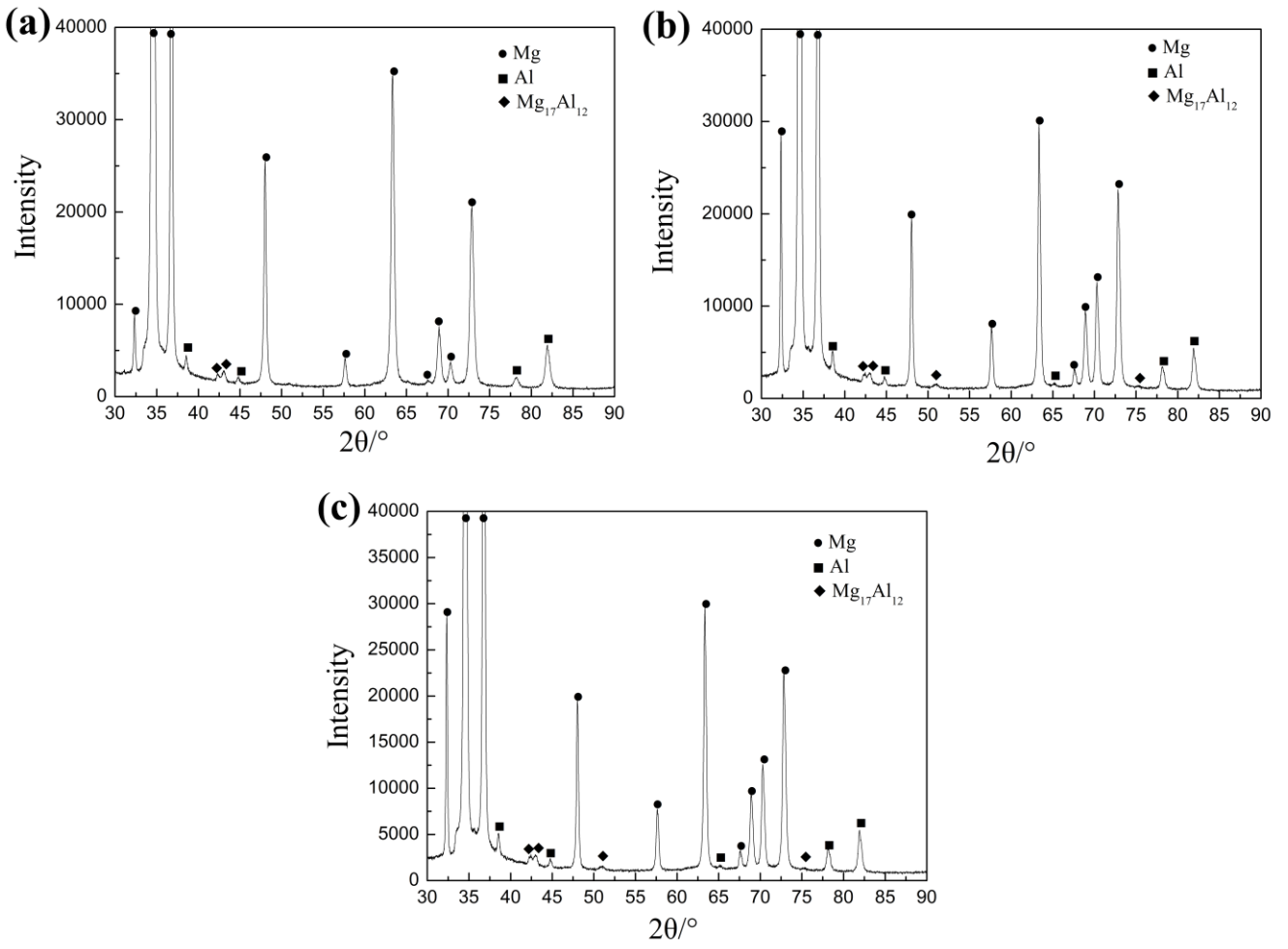


**Figure 8.** XRD results of the 10 wt.% $H_3PO_4$ etched samples (a) without annealing, (b) with annealing at 200 °C for 1 h, (c) with annealing at 400 °C for 1 h

Fig. 8(a)-(c) show the XRD results of the 10 wt.% $H_3PO_4$ etched samples without annealing, with annealing at 200 °C for 1 h and with annealing at 400 °C for 1 h, respectively. The signal of Mg in Fig. 8(a)-(c) is high because the thickness of the aluminum coating is small. As can be seen from

Fig. 8(a)-(c), the 2θ signals located at 38.5°, 44.7°, 65.8°, 78.3° and 82° correspond to the (111), (200), (220), (311) and (222) crystal planes in the FCC Al, respectively (JCPDS No. 00-004-0787). The peak of the signals in Fig. 8(b)-(c) is shaper than that in Fig. 8 (a), which indicates that the crystallinity of Al is better compared with the sample without annealing and this is also in accordance with the morphology shown in SEM images. The samples with annealing in Fig. 8(b)-(c) show higher signals and more crystallographic orientations of $Mg_{17}Al_{12}$ compared with the unannealed sample in Fig. 8 (a), which can be ascribed to the enhanced diffusion of Al to the magnesium alloy substrate and the formation of more $Mg_{17}Al_{12}$ phase. However, $Mg_2Al_3$ phase cannot be observed. The results agree well with the conclusion from Wu et al. and Huo et al. who claimed that Al film reacted completely with the AZ91D magnesium alloy substrate to form $Mg_{17}Al_{12}$ phase after heat treatment in a high vacuum and no $Mg_2Al_3$ phase was observed [34, 48].

*3.3.2 Influence of annealing process on adhesive strength and corrosion resistance*

The effect of the annealing process on the adhesive strength between the coating and the substrate is shown in Table 4, the pretreatment process is chosen as etching with 10 wt.% $H_3PO_4$. It's obvious that the adhesive strength improves with the annealing treatment as well as the annealing temperature. The sample annealed at 400 °C for 1 h shows the best adhesive strength.

**Table 4.** Adhesive strength of the Al coatings under different annealing processes

| Treatment | Percentage of grid area removed | Grade |
|---|---|---|
| unannealed | 21% | 2B |
| annealing at 200 °C for 1 h | 13% | 3B |
| annealing at 400 °C for 1 h | 5% | 4B |

Fig. 9(a), (b) show the AC impedance curves and Tafel curves of the 10 wt.% $H_3PO_4$ etched samples without annealing, with annealing at 200 °C for 1 h and with annealing at 400 °C for 1 h, respectively. We can tell from Fig. 9(a), (b) that annealing process doesn't necessarily improve the corrosion resistance of the coating. As can be seen from the AC impedance curves in Fig. 9(a), the smallest diameter of the capacitive loop corresponds to the sample after annealing at 400 °C for 1 h which represents the worst corrosion resistance. The corrosion current density of the samples derived from the Tafel curves in Fig. 9(b) increases from $4.4\times10^{-5}$ A $cm^{-2}$ to $7.2\times10^{-5}$ A $cm^{-2}$ and finally to $1.7\times10^{-4}$ A $cm^{-2}$ without annealing, with annealing at 200 °C for 1 h and with annealing at 400 °C for 1 h, respectively. The corresponding polarization resistance also decreases from 440.6 Ω to 291.8 Ω and finally to 157.8 Ω accordingly. Li et al. [38] also found out that the annealing treatment lowered the magnesium alloy's corrosion resistance. The typical microstructure of AZ91D magnesium alloy

contains a matrix of α-Mg grains and a divorced eutectic composed of secondary α-Mg and the $Mg_{17}Al_{12}$ phase [49]. The fact that the corrosion resistance of the samples decreases with the annealing process can be ascribed to the following [49]: The corrosive performance of the AZ91D alloy is determined by the composition, grain size, amount and distribution of $Mg_{17}Al_{12}$ phase. The $Mg_{17}Al_{12}$ phase can act either as a barrier to corrosion or as a galvanic cathode depending on the microstructure. When the fraction of $Mg_{17}Al_{12}$ phase is relatively high and $Mg_{17}Al_{12}$ phase is distributed continuously, the $Mg_{17}Al_{12}$ phase is expected to act as a barrier to corrosion, just as Huo et al. claimed that the corrosion resistance of the AZ91D magnesium alloy increased after annealing owing to a large amount of continuously distributed $Mg_{17}Al_{12}$ phase [48]. However, accelerated corrosion due to microgalvanic corrosion is expected when the fraction of $Mg_{17}Al_{12}$ phase is smaller and sparsely distributed. Whether annealing or not, the amount of $Mg_{17}Al_{12}$ phase is rather scarce, which acts as a galvanic cathode, thus accelerating the overall corrosion of the α matrix, so the corrosion resistance decreases with more $Mg_{17}Al_{12}$ phase generated by the annealing process.

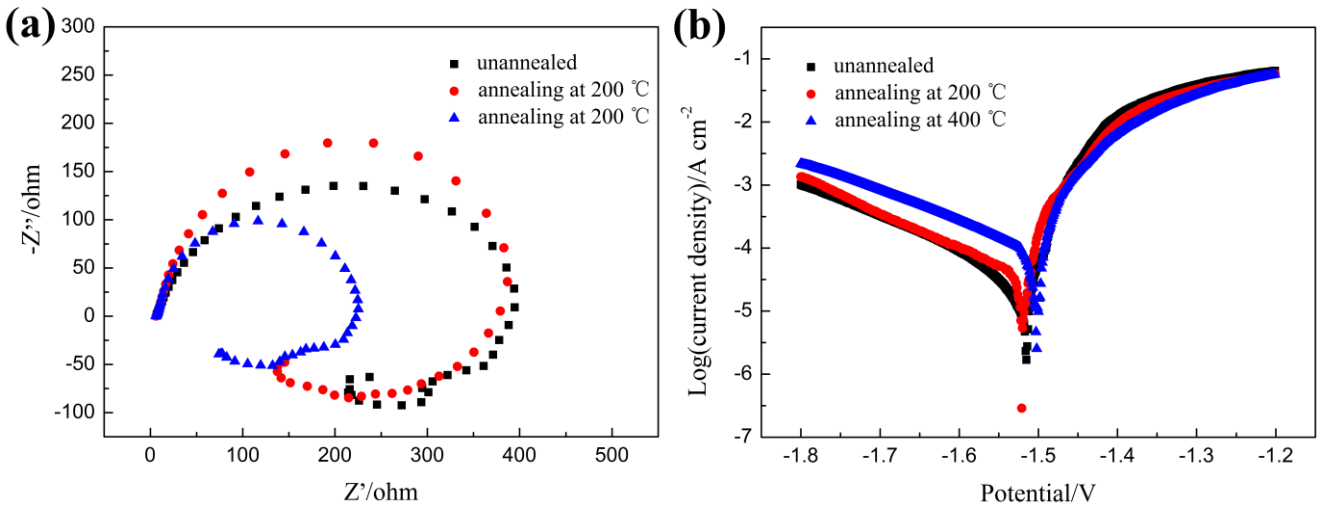


**Figure 9.** (a) AC impedance curves, (b) Tafel curves of the 10 wt.% $H_3PO_4$ etched samples without annealing, with annealing at 200 °C for 1 h and with annealing at 400 °C for 1 h

## 4. CONCLUSIONS

In summary, vacuum evaporation deposition was used to successfully prepare an aluminum coating on AZ91D magnesium alloy in an attempt to enhance the corrosion resistance of magnesium alloys. The effect of pretreatment of the substrate, deposition time and annealing treatment on the surface morphology, corrosion resistance and adhesive strength of the coating were systemically investigated. The results indicate that the best corrosion resistance after deposition of aluminum is obtained for the sample pretreated by $H_3PO_4$ etching. The corrosion resistance is increased significantly after deposition and the corresponding aluminum coating shows the highest adhesive strength. As the deposition time increases from 3 min to 6 min and finally to 9 min, a continuous and dense aluminum coating gradually forms on the surface of the magnesium alloy substrate following the typical island growth (Volmer-Weber) mode. The increase of deposition time enhances the corrosion

resistance of magnesium alloy but has no effect on the adhesive strength between the coating and the substrate. With the increase of the annealing temperature, the coating of the sample becomes more uniform with better crystallinity of aluminum compared with unannealed sample. The adhesive strength increases, whereas the corrosion resistance declines.

ACKNOWLEDGEMENT
This work was supported by the National Nature Science Foundation of China (51374005 and 51004070) and National Key Technology R&D Program of China (2011BAE13B08).

**References**

1. H. Hoche, J. Schmidt, S. Groß, T. Troßmann, C. Berger, *Surf. Coat. Technol.*, 205 (2011) S145.
2. H. Hoche, C. Blawert, E. Broszeit, C. Berger, *Surf. Coat. Technol.*, 193 (2005) 223.
3. Y. Zhang, S. Wu, Q. Chen, X. Zhou, Z. Wei, *Int. J. Electrochem. Sci.*, 10 (2015) 1015.
4. T. Tanski, K. Labisz, K. Lukaszkowicz, A. Sliwa, K. Golombek, *Surf. Eng.*, 30 (2014) 927.
5. M. Daroonparvar, M.A.M. Yajid, N.M. Yusof, H.R. Bakhsheshi-Rad, E. Hamzah, H.A. Kamali, *J. Alloy. Compd.*, 615 (2014) 657.
6. M.E. Ikpi, J. Dong, W. Ke, *Int. J. Electrochem. Sci.*, 10 (2015) 552.
7. C. Man, C. Dong, Y. Fang, K. Xiao, C. Guo, G. He, X. Li, *Int. J. Electrochem. Sci.*, 10 (2015) 8691.
8. R. C. Zeng, J. Zhang, W. J. Huang, W. Dietzel, K. Kainer, C. Blawert, K. Wei, *T. Nonferr. Metal Soc.*, 16 (2006) S763.
9. H. Altun, H. Sinici, *Mater. Charact.*, 59 (2008) 266.
10. G.S. Wu, X.Q. Zeng, G.Y. Yuan, *Mater. Lett.*, 62 (2008) 4325.
11. D. Wu, X. Liu, K. Lu, Y. Zhang, H. Wang, *Appl. Surf. Sci.*, 255 (2009) 7115.
12. A. Ghasemi, V. Raja, C. Blawert, W. Dietzel, K. Kainer, *Surf. Coat. Technol.*, 204 (2010) 1469.
13. Z. Qiu, R. Wang, X. Wu, Y. Zhang, *Int. J. Electrochem. Sci.*, 8 (2013) 1957.
14. X. Tu, L. Chen, J. Shen, Y. Zhang, C. Miao, J. Wu, *Int. J. Electrochem. Sci.*, 7 (2012) 9573.
15. W. Zhou, D. Shan, E.-H. Han, W. Ke, *Corros. Sci.*, 50 (2008) 329.
16. A.R. Shashikala, R. Umarani, S.M. Mayanna, A.K. Sharma, *Int. J. Electrochem. Sci.*, 3 (2008) 993.
17. Y. Su, G. Li, J. Lian, *Int. J. Electrochem. Sci.*, 7 (2012) 11497.
18. I. Shigematsu, M. Nakamura, N. Saitou, K. Shimojima, *J. Mater. Sci. Lett.*, 19 (2000) 473.
19. C. Zhong, M.F. He, L. Liu, Y.J. Chen, B. Shen, Y.T. Wu, Y.D. Deng, W.B. Hu, *Surf. Coat. Technol.*, 205 (2010) 2412.
20. C. Zhong, M.F. He, L. Liu, Y.T. Wu, Y.J. Chen, Y.D. Deng, B. Shen, W.B. Hu, *J. Alloy. Compd.*, 504 (2010) 377.
21. C. Zhong, F. Liu, Y.T. Wu, J.J. Le, L. Liu, M.F. He, J.C. Zhu, W.B. Hu, *J. Alloy. Compd.*, 520 (2012) 11.
22. J.J. Le, L. Liu, F. Liu, Y.D. Deng, C. Zhong, W.B. Hu, *J. Alloy. Compd.*, 610 (2014) 173.
23. J.W. Tang, K. Azumi, *Surf. Coat. Technol.*, 208 (2012) 1.
24. B.J. Xu, M. Zhang, G.P. Ling, *Surf. Coat. Technol.*, 239 (2014) 1.
25. M. Ueda, S. Hariyama, T. Ohtsuka, *J. Solid. State. Electr.*, 16 (2012) 3423.
26. E.A.M. Husain, A. Husain, A. Abdel Nazeer, J.M. Al-Saraf, K. Al-Awadhi, A. Shekeban, M. Murad, *Int. J. Electrochem. Sci.*, 10 (2015) 5194.
27. F. Liu, Y.D. Deng, X.P. Han, W.B. Hu, C. Zhong, *J. Alloy. Compd.*, 654 (2016) 163.
28. H. Ye, X.B. Zhang, X. Chang, R. Chen, *Manufacturing Process Technology, Pts 1-5*, 189-193 (2011) 867.
29. P.H. Gao, J.P. Li, Z. Yang, Y.C. Guo, Y.R. Wang, *Light Metals Technology 2013*, 765 (2013) 639.
30. B. Navinšek, P. Panjan, I. Milošev, *Surf. Coat. Technol.*, 97 (1997) 182.
31. H.A. Jehn, B. Rother, *Surf. Coat. Technol.*, 112 (1999) 103.

32. G.S. Wu, *Mater. Lett.*, 61 (2007) 3815.
33. G.S. Wu, X.Q. Zeng, S.S. Yao, X.M. Wang, *Mater. Lett.*, 61 (2007) 4019.
34. S. Wu, S. Yen, T. Chou, *Surf. Coat. Technol.*, 200 (2006) 2769.
35. E. Zhang, L. Xu, K. Yang, *Scr. Mater.*, 53 (2005) 523.
36. A. Yamamoto, A. Watanabe, K. Sugahara, H. Tsubakino, S. Fukumoto, *Scripta Mater.*, 44 (2001) 1039.
37. B. L. Yu, J. Y. Uan, *Scripta Mater.*, 54 (2006) 1253.
38. L. Li, R. He, G.J. Huang, S.S. Xie, *Adv. Mater. Res-Switz.*, 213 (2011) 497.
39. H.W. Huo, Y. Li, F.H. Wang, *J. Mater. Sci. Technol.*, 23 (2007) 379.
40. D.Y. Hwang, Y.G. Ko, Y.M. Kim, B. Yoo, D.H. Shin, *Mater. Trans.*, 51 (2010) 408.
41. N. Iranipour, R.A. Khosroshahi, N.P. Ahmadi, *Surf. Coat. Technol.*, 205 (2010) 2281.
42. ASTM D3359. "Standard Test Methods for Measuring Adhesion by Tape Test." (2005).
43. K. Brunelli, M. Dabala, I. Calliari, M. Magrini, *Corros. Sci.*, 47 (2005) 989.
44. H. H. Elsentriecy, K. Azumi, H. Konno, *Surf. Coat. Technol.*, 202 (2007) 532.
45. R. Supplit, T. Koch, U. Schubert, *Corros. Sci.*, 49 (2007) 3015.
46. J.A. Floro, E. Chason, R.C. Cammarata, D.J. Srolovitz, *MRS. bull.*, 27 (2002) 19.
47. M. Evans, J. Glueckstein, J. Nogami, *Phys. Rev. B.*, 53 (1996) 4000.
48. H. W. Huo, F. H. Wang, Y. Li, J. Y. Xu, *Corros. Sci. Protect. Technol.*, 13 (2001) 484.
49. G. Song, A. Atrens, M. Dargusch, *Corros. Sci.*, 41 (1998) 249.